

Entropy of a restricted primitive model electrolyte using a mean electrostatic potential approach

S. Lamperski ¹, L. B. Bhuiyan ², C. W. Outhwaite ³, R. Gorniak ¹

¹ Faculty of Chemistry, Adam Mickiewicz University in Poznań, Uniwersytetu Poznańskiego 8, 61-614 Poznań, Poland

² Laboratory of Theoretical Physics, Department of Physics, University of Puerto Rico, 17 Avenida Universidad, STE 1701, San Juan, Puerto Rico 00925-2537, USA

³ School of Mathematical and Physical Sciences, University of Sheffield, Sheffield S3 7RH, UK

Received November 21, 2024, in final form February 11, 2025

The excess entropy of restricted primitive model electrolytes is calculated using a potential based approach through the symmetric Poisson-Boltzmann and the modified Poisson-Boltzmann theories. The theories are utilized in conjunction with a statistical thermodynamics equation that is shown to be equivalent to thermodynamic integration. Electrolyte systems having ionic valencies 1:1 and 2:2 with diameters 3×10^{-10} m and 4.25×10^{-10} m are treated over a wide range of concentrations. The exact radial distribution functions for the model electrolytes obtained from Monte Carlo simulations in the canonical ensemble are compared with the corresponding theoretical predictions. Furthermore, the radial distribution functions from the theories and the simulations are used in the Laird-Haymet entropy expansion equations [J. Chem. Phys., 1994, **100**, 3775] to estimate the excess entropy of the solutions. These equations take into account multi-particle distribution functions, which are approximated using a “ring” term. In general, the modified Poisson-Boltzmann theory gives results that are more consistent with the simulation data than those from the symmetric Poisson-Boltzmann theory. The results show that the excess entropy is negative with its absolute value increasing for 1:1 electrolytes with increasing concentration. The symmetric Poisson-Boltzmann values are slightly overestimated, while the modified Poisson-Boltzmann values are slightly underestimated relative to the simulations. The curves for 1:1 electrolytes including that from the Laird-Haymet equations are consistent with each other, while only the MPB curves for 2:2 electrolytes at 4.25×10^{-10} m are qualitative relative to the simulations up to about 1 mol/dm³. The 2:2 electrolyte curves reveal a characteristic inflection and plateau. The results obtained in the low concentration range (< 0.01 mol/dm³) are consistent with the predictions of the Debye-Hückel limiting law.

Key words: *electrolytes, restricted primitive model, entropy, thermodynamic integration, Monte Carlo simulations, symmetric and modified Poisson-Boltzmann theories*

1. Introduction

The concept of entropy is arguably one of the most intriguing ones in statistical thermodynamics. The pioneering work in relating Clausius thermodynamic entropy S to the probabilistic description of the microscopic distributions of the molecules in a system was done by Boltzmann [1] reflected in his famous equation

$$S = k_B \ln W, \quad (1)$$

where W is the number of available microstates with k_B being the Boltzmann’s constant. This equation is equivalent to

$$S = -k_B \sum_r p_r \ln p_r, \quad (2)$$

where p_r is the probability of a distribution [2]. The concept has found its way to other areas of modern science, for example, Shannon's entropy [3] in information theory has the same form as equation (2) with analogous interpretation. Our interest in this work is more modest and we will be focusing on the entropy of charged fluids. Entropy is one of the more important thermodynamic functions in such systems, which is perhaps as significant as the osmotic and activity coefficients are in characterizing the equilibrium properties. A standard, traditional method of calculating entropy S is through thermodynamic integration (TI) [4, 5]. We will show (in the next section) that the TI is equivalent to a known equation in statistical thermodynamics relating the excess free energy $F^{(\text{ex})}$, the osmotic coefficient ϕ , and the mean activity coefficients γ_{\pm} . The use of the defining thermodynamic relation for the free energy then yields the entropy.

Our second approach to estimating S is through the radial distribution functions of the electrolytes. The Boltzmann equation can also be expressed in terms of a partition function, and hence can be related to the distribution of the constituent species. In the case of liquids, an early work in this respect is due to Green [6] whose proposed equations turned out to be useful. These equations involve second order (radial) and higher order distribution functions. Subsequently, Laird and Haymet used them to calculate the excess entropy of hard spheres [7]. The contribution of higher order distribution functions was approximated using a partial summation, the so-called 'ring' method developed by Hernando [8, 9]. Very good agreement for entropy was obtained relative to that from an exact expression emanating from the Percus-Yevick (PY) approximation for hard spheres [5]. For electrolytes also, as in the case of hard spheres, Laird and Haymet [10] approximated the entropy expansion up to the 'ring' term. Although the equations developed by Laird and Haymet have some limitations, they represent an important step towards using distribution functions to calculate the entropy of liquids and electrolytes. Silverstein, Dill and Haymet investigated the solvation entropy using multi-molecular entropy expansion [11]. Lazaridis dealt with solvation entropy, but in heterogeneous liquids and low concentrations [12]. It is also worth noting the work of Lazaridis and Karplus [13], who, in addition to the radial distribution function, used an indicative distribution function, which was a function of 5 angles, to describe the entropy of pure water. Recently, Hernando and Blum proposed a new entropy component, which is related to density fluctuations [14]. At the other end of the concentration scale, we have very dilute electrolytes. Their chemical potential is described by the well-known Debye-Hückel limiting law (DHLL). Based on this law, Laird and Haymet derived formulas for the limiting excess entropy and its components [10]. The hypernetted chain (HNC) [4, 15, 16] approximation has also been used to calculate the electrolyte entropy.

In this study we will employ the symmetric Poisson-Boltzmann (SPB) and the modified Poisson-Boltzmann (MPB) theories along with Monte Carlo (MC) simulations to evaluate the ϕ , γ_{\pm} , the energy U , and hence the S . We will also use the mean spherical approximation (MSA) for comparison purposes. With regard to the alternative approach, we will utilize the radial distribution profiles from the SPB, MPB, and the simulations together with the LH expressions [10] to calculate S . In the rest of the paper we will refer to the former procedure as TI and the latter as LH approximation. Symmetric valency 1:1 and 2:2 electrolytes will be treated for two different ionic sizes and for a range of concentrations. The SPB and MPB are potential based approaches and had earlier proved to be valuable in characterizing structural and thermodynamic properties of electrolytes and electrolyte mixtures including colloidal solutions [17–21]. The MSA, on the other hand, is a well known integral equation theory with the advantage of being analytically tractable [5]. These theories have, however, not been previously applied to a calculation of entropy of electrolytes. It is of interest to examine the viability of these approaches in estimating the entropy in such systems. The SPB and MPB results will afford useful comparative assessment of the two approaches vis-à-vis the simulations.

2. Model and methods

2.1. The model

The physical model of the electrolyte used in this work is the restricted primitive model (RPM). The ions are depicted as equi-sized charged hard spheres in a structureless solvent approximated by a continuum dielectric characterized by a dielectric constant ϵ_r . In the Hamiltonian, the pairwise additive

interaction potential between two ions i and j separated by a distance r is given by

$$u_{ij}(r) = \begin{cases} \infty, & r < d, \\ e^2 Z_i Z_j / (4\pi\epsilon_0\epsilon_r r), & r > d, \end{cases} \quad (3)$$

where Z_i is the valency of ion i , ϵ_0 is the vacuum permittivity, d is the common ionic diameter, and e is the absolute value of the fundamental charge. We have further used symmetric 1:1 and 2:2 valencies and $d = 3 \times 10^{-10}$ m or 4.25×10^{-10} m. The temperature T and the relative permittivity ϵ_r were held constant at 298.15 K and 78.5, respectively.

2.2. The equivalence of thermodynamic integration with an equation in statistical thermodynamics

Using TI to calculate S involves the calculation of the excess free energy $F^{(\text{ex})}$ by integrating the energy U . In a charged fluid system in equilibrium, U is simply the configurational potential energy. For example, the electrical part of the free energy can be written [5, 17]

$$F^{\text{el}} = \sum_i e_i \rho_i \int_0^1 d\lambda \psi'_i(\lambda), \quad (4)$$

where ρ_i is the mean number density of ion species i , and

$$\psi'_i = \lim_{\lambda \rightarrow 1} \left[\psi_i(r_{12}) - \frac{e_i}{4\pi\epsilon_0\epsilon_r r_{12}} \right], \quad (5)$$

is the potential at the centre of ion i at \mathbf{r}_1 due to all other ions, $\psi_i(r_{12})$ is the mean electrostatic potential at \mathbf{r}_2 given ion i at \mathbf{r}_1 and $e_i = eZ_i$. The quantity λ is the charging parameter such that the charge of each ion of type i at any stage of the charging process is λe_i , where $0 \leq \lambda \leq 1$ (Debye charging process).

From thermodynamics we have

$$\frac{1}{\beta} \ln \gamma_i^{\text{el}} = \frac{\partial F^{\text{el}}}{\partial \rho_i} = e_i \int_0^1 d\lambda \psi'_i(\lambda), \quad (6)$$

where γ_i^{el} is the electrical part of the individual activity coefficient and $\beta = 1/(k_B T)$. Taking $i, j = +, -$, we get from equations (4) and (6)

$$\ln \gamma_{\pm}^{\text{el}} = \frac{\beta}{\rho} \sum_i \rho_i \frac{\partial F^{\text{el}}}{\partial \rho_i}, \quad (7)$$

with the total number density of ions $\rho = \sum_i \rho_i$ and γ_{\pm}^{el} , the electrical contribution to the mean activity coefficient defined through

$$\ln \gamma_{\pm}^{\text{el}} = \frac{1}{\rho} \sum_i \rho_i \ln \gamma_i^{\text{el}}. \quad (8)$$

This is indeed a general definition of the mean activity coefficient (starting from the individual activity coefficients).

Consider now the thermodynamic expressions relating the excess osmotic coefficient $\phi^{\text{ex}} (= \phi - 1)$, the activity coefficient γ_i , and the excess free energy F^{ex}

$$\phi^{\text{ex}} = -\frac{\beta F^{\text{ex}}}{\rho} + \frac{\beta}{\rho} \sum_i \rho_i \left(\frac{\partial F^{\text{ex}}}{\partial \rho_i} \right), \quad (9)$$

$$\ln \gamma_i = \beta \left(\frac{\partial F^{\text{ex}}}{\partial \rho_i} \right). \quad (10)$$

Equations (9) and (10) lead directly to the statistical thermodynamics equation

$$\phi^{\text{ex}} = -\frac{\beta F^{\text{ex}}}{\rho} + \ln \gamma_{\pm}. \quad (11)$$

A similar equation has been used by Ruas et al. [22] using the binding MSA. Alternatively if the excess properties can be written as the sum of the electrical and non-electrical parts, then equation (11) follows from equations (7), (9) and (10).

Combining equation (11) with the thermodynamic definition of free energy, that is, $F = U - TS$, yields an expression for the excess entropy in the solution.

$$\frac{S^{(\text{ex})}}{\rho k_B} = \frac{\beta U}{\rho} - \ln \gamma_{\pm} + \phi^{\text{ex}}. \quad (12)$$

The left hand side of the above equation represents excess entropy per particle, while the first term on the right hand side is the reduced energy per particle. This equation is just another representation of TI. In passing, it is noted that in the MSA for a PM, the thermodynamic quantities such as ϕ , $\ln \gamma_{\pm}$, and U have closed analytical forms [23–25], which is useful for a quick analysis of experimental data.

2.3. The SPB and MPB theories

The symmetric Poisson-Boltzmann and the modified Poisson-Boltzmann theories are both potential based statistical mechanical approaches to the theory of bulk electrolytes. The details of the development of these theories have been chronicled elsewhere in the literature [26–31]. We will restrict ourselves here to outlining the salient features of the theories along with the relevant equations. As the term “symmetric” indicates, the SPB originates in the efforts, initially by [26, 27] and later by Outhwaite and co-workers [28–31], to symmetrize the radial distribution function $g_{ij}(r)$ of the conventional non-linear Poisson-Boltzmann (PB) theory with respect to an interchange of indices, that is, $g_{ij}(r) = g_{ji}(r)$ for asymmetric systems. In the SPB theory, the $g_{ij}(r)$ reads

$$g_{ij}(r) = g_{ij}^0(r) \exp \left\{ -\frac{\beta e}{2} \left[Z_i(\psi_j(r) + \psi_j^0(r)) + Z_j(\psi_i(r) + \psi_i^0(r)) \right] \right\}. \quad (13)$$

Here $\psi_i(r)$ is the mean electrostatic potential about an ion of species i at a distance r , while $\psi_i^0(r) = \psi_i(r; Z_i = 0)$ is the corresponding discharged potential. The discharged potentials are zero for a RPM system so that the equation simplifies to

$$g_{ij}(r) = g_{ij}^0(r) \exp \left\{ -\frac{\beta e}{2} \left[Z_i \psi_j(r) + Z_j \psi_i(r) \right] \right\}. \quad (14)$$

The quantity $g_{ij}^0(r) = g_{ij}(r; Z = Z_i = 0)$ is the exclusion volume term and is the radial distribution function between the two discharged ions in a sea of fully charged ions. The SPB theory for the RPM is completed by combining equation (14) with Poisson’s equation

$$\nabla^2 \psi_i(r) = -\frac{e}{\epsilon_0 \epsilon_r} \sum_j Z_j \rho_j g_{ij}(r). \quad (15)$$

The SPB has a mean field character although $g_{ij}^0(r)$ does contain short-range hard-core effects. The main inter-ionic correlations occur in the neglected fluctuation potential which incorporates both the short-range and coulombic long-range contributions.

The fluctuation potentials, missing in the SPB theory, are accounted for in the MPB theory [29–31], where the $g_{ij}(r)$ now transforms to

$$g_{ij}(r) = g_{ij}^0(r) \exp \left\{ -\frac{\beta e}{2} \left[Z_i L_i(u_j) + Z_j L_j(u_i) \right] \right\}, \quad (16)$$

where

$$L_i(u_j) = \frac{1}{2r(1 + \kappa d)} \left\{ u_j(r + d) + u_j(r - d) + \kappa \int_{r-d}^{r+d} dr u_j(r) \right\}, \quad (17)$$

$$\kappa = \left[\frac{\beta e^2}{\epsilon_0 \epsilon_r} \sum_i Z_i^2 \rho_i \right]^{\frac{1}{2}}. \quad (18)$$

Here, κ is the Debye-Hückel constant and $u_i(r) = r\psi_i(r)$. The equations (15)–(18) are the MPB equations for a RPM electrolyte.

In both the SPB and MPB theories, the $g_{ij}^0(r)$ were taken to be given by the Percus-Yevick (PY) hard sphere radial distribution functions with Verlet-Weis (VW) corrections [32]. This has proved successful in many previous applications of these theories to different electrolytes [33, 34].

2.4. Monte Carlo simulations

MC simulations were performed to obtain the internal energy $U/(\rho k_B T)$ and the osmotic coefficient ϕ in the canonical ensemble, while the mean activity coefficient γ_{\pm} was calculated in the inverse grand canonical (IGCMC) ensemble [35], with the standard Metropolis algorithm being utilized in both cases. Periodic boundary conditions and the minimum image convention were applied in all three directions. In the canonical ensemble, the number of ions N is constant, while for IGCMC it fluctuates. In both cases equilibration runs were set between $(1 - 30) \times 10^7$ steps while the production runs consisted of $(1 - 10) \times 10^8$ configurations. The interactions between ions were described by equation (3), which includes both hard-sphere and electrostatic interactions.

The radial distribution function $g_{ij}(r)$ can be generated using molecular computer simulations. The results obtained are exact for the considered model and can serve as a reference point for assessing an approximate theory. In statistical thermodynamics, $g_{ij}(r)$ is defined as the probability of finding a molecule j located at a distance r from a molecule i , called the central one. This definition is mathematically described by the equation

$$g_{ij}(r) = \frac{dN_j(r)}{dV(r)\rho_j}, \quad (19)$$

where dN_j is the average number of molecules j in a spherical shell with radius r , thickness dr and volume dV . In computer simulations, $g_{ij}(r)$ is calculated from the above formula. A typical algorithm can be found in the Frenkel and Smit textbook [36]. The calculations were carried out for a wide range of electrolyte concentrations from 0.001 mol/dm³ to 6.76 mol/dm³. The canonical ensemble simulations utilized 5000 ions at low concentrations with a step-length (in units scaled with respect to the side length of the simulation box) close to unity. However, at high concentrations, these values were 2000 and 0.05, respectively. Large numbers of ions ensured that the $g_{ij}(r)$ functions converged to 1 at large distances, which is a necessary condition to obtaining correct entropy data.

2.5. Laird-Haymet entropy expansions

The pair distributions $g_{ij}(r)$'s obtained from the MC, SPB, and MPB theories were used in the entropy expansion, in terms of multi-particle correlations, developed initially by Hernando [8, 9] and later by Laird and Haymet [10] to calculate the entropy. The LH formalism entails calculation of the quantities $S^{(2)}$, S_{ring} , both of which involve pair correlations, with the excess entropy being written as

$$S^{(\text{ex})} = S^{(2)} + S_{\text{ring}}, \quad (20)$$

the two terms on the right-hand side being the second and third terms in the entropy expansion. In particular, S_{ring} may be taken to be an indirect contribution of higher order terms.

For completeness, we quote here the specific expressions for $S^{(2)}$ and S_{ring} [10] using the present notations:

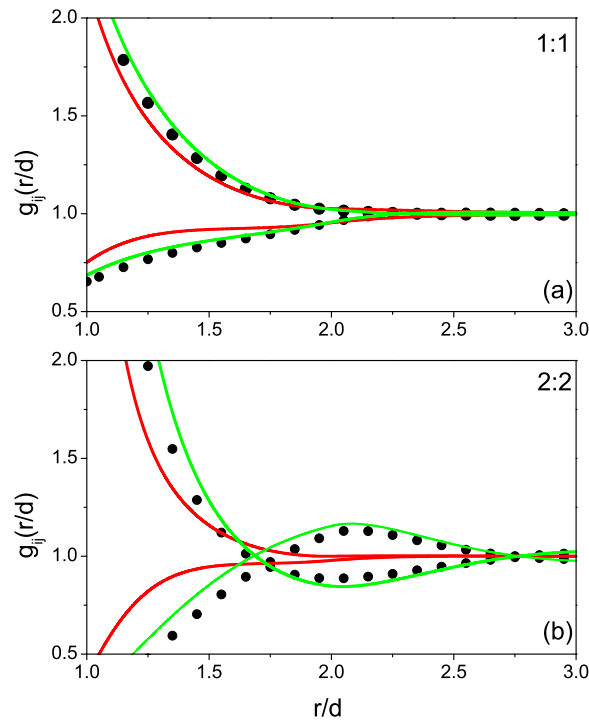


Figure 1. (Colour online) Radial distribution function, $g_{ij}(r/d)$ as a function of r/d for a RPM electrolyte, $d = 4.25 \times 10^{-10}$ m, $c = 1.96$ mol/dm³, $T = 298.15$ K, and $\epsilon_r = 78.5$. Legend: SPB (red lines), MPB (green lines), and MC (black filled circles). Panel (a) 1:1 valency, panel (b) 2:2 valency.

$$S^{(2)} = -\frac{1}{2\rho} \sum_i \sum_j \rho_i \rho_j \int d\mathbf{r}_{ij} [g_{ij}(r_{ij}) \ln g_{ij}(r_{ij}) - g_{ij}(r_{ij}) + 1], \quad (21)$$

and

$$S_{\text{ring}} = \frac{1}{2\rho(2\pi)^3} \int d\mathbf{k} \left[\ln |\mathbf{I} + \tilde{\mathbf{H}}(k)| + \frac{1}{2} \text{Tr} \left(\tilde{\mathbf{H}}^2(k) \right) - \text{Tr} \left(\tilde{\mathbf{H}}(k) \right) \right]. \quad (22)$$

Here, \mathbf{H} and \mathbf{I} are 2×2 matrices, with the latter being the identity matrix.

$$\tilde{\mathbf{H}}(k)_{ij} = \rho_i^{1/2} \rho_j^{1/2} \tilde{h}_{ij}(k), \quad (23)$$

where $\tilde{h}_{ij}(k)$ is the Fourier transform of $h_{ij}(r) = g_{ij}(r) - 1$, and for an isotropic, homogeneous fluid, $\tilde{h}_{ij}(k)$ can be written as

$$\tilde{h}_{ij}(k) = 4\pi \int_0^\infty dr r^2 \{g_{ij}(r) - 1\} \frac{\sin kr}{kr}. \quad (24)$$

For numerical integration purposes, the right-hand sides of equations (21) and (22) were expanded and cast in the following forms. For example, after expanding the right-hand side of equation (21), it can be written as

$$S^{(2)} = I_1 + I_2 + I_3, \quad (25)$$

$$I_1 = -3\eta \int_0^\infty dr_{ii}^* (r_{ii}^*)^2 \{g_{ii}(r^*) \ln g_{ii}(r^*) - g_{ii}(r^*) + 1\}, \quad (26)$$

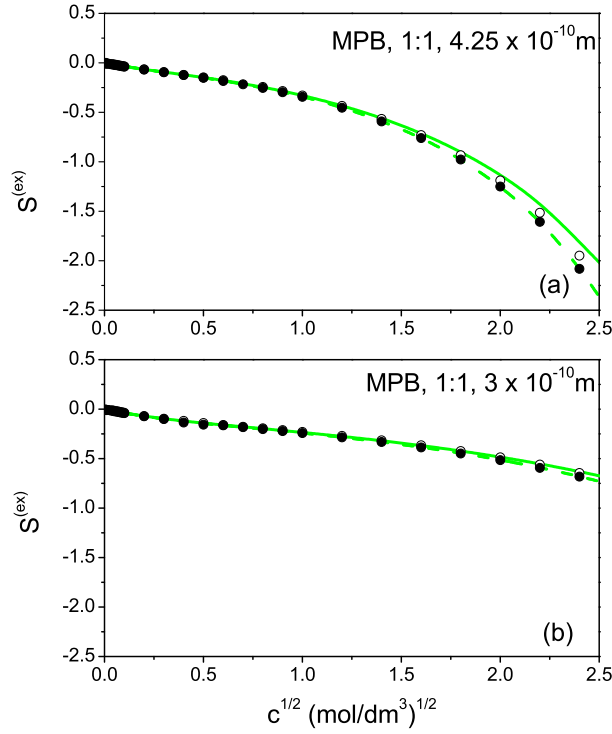


Figure 2. (Colour online) Excess entropy $S^{(ex)}$ as a function of the square root of electrolyte concentration for a 1:1 valency RPM electrolyte. Legend: MPB_{TI} (solid green lines), MPB_{LH} (dashed green lines), MC_{TI} (black filled), and MC_{LH} (black open circles). Panel (a) $d = 4.25 \times 10^{-10}$ m, Panel (b) $d = 3 \times 10^{-10}$ m. The SPB and MPB predictions are only distinguishable on the graphical scale at the highest concentrations. The remaining RPM parameters as in figure 1.

$$I_2 = -6\eta \int_0^{\infty} dr_{ij}^* (r_{ij}^*)^2 \{g_{ij}(r^*) \ln g_{ij}(r^*) - g_{ij}(r^*) + 1\}, \quad (27)$$

I_3 is now obtained from I_1 simply by the interchange $i \leftrightarrow j$. In the above equations, $\eta = \frac{\pi}{6} \rho a^3$ is the total packing fraction, and $r^* = r/a$. Defining further, $y = ka$, and $M_{ij}(k) = \tilde{h}_{ij}(k)/a^3$, equation (22) becomes

$$S_{\text{ring}} = I_4 + I_5 + I_6, \quad (28)$$

$$I_4 = \frac{1}{24\pi\eta} \int_0^{\infty} dy y^2 \ln \left\{ 1 + \left(\frac{6\eta}{2\pi} \right)^2 M_{ii} M_{jj} + \left(\frac{6\eta}{2\pi} \right) (M_{ii} + M_{jj}) - \left(\frac{6\eta}{2\pi} \right)^2 M_{ij}^2 \right\}, \quad (29)$$

$$I_5 = \frac{1}{24\pi\eta} \int_0^{\infty} dy y^2 \left\{ \frac{1}{2} \left(\frac{6\eta}{2\pi} \right)^2 (M_{ii}^2 + 2M_{ij}^2 + M_{jj}^2) \right\}, \quad (30)$$

and

$$I_6 = -\frac{1}{24\pi\eta} \int_0^{\infty} dy y^2 \left(\frac{6\eta}{2\pi} \right) (M_{ii} + M_{jj}). \quad (31)$$

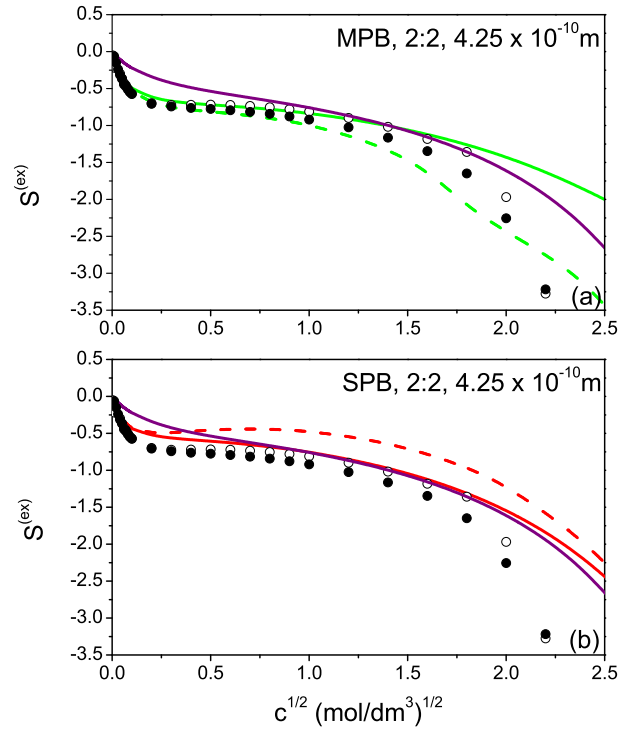


Figure 3. (Colour online) Excess entropy $S^{(\text{ex})}$ as a function of the square root of electrolyte concentration for a 2:2 valency RPM electrolyte, $d = 4.25 \times 10^{-10}$ m. Legend: panel (a) MPB_{TI} (solid green lines), MPB_{LH} (dashed green lines), MSA_{TI} (purple line), MC_{TI} (black filled circles), and MC_{LH} (black open circles). Panel (b) SPB_{TI} (solid red lines), SPB_{LH} (dashed red lines), MSA_{TI} (purple line), MC_{TI} (black filled circles), and MC_{LH} (black open circles). The remaining RPM parameters as in figure 1.

The SPB, MPB, or MC results for $S^{(2)}$, S_{ring} , and hence $S^{(\text{ex})}$ are now obtained by using the relevant pair correlation functions g_{ij} in the expressions for $I_1 - I_6$ with the integrals being evaluated by using the Simpson rule. As a check on the numerics we could reproduce some of the results in table 1 of reference [7] for a pure hard sphere fluid with the g_{ij} given by the PY + VW theories.

Using the HNC equation, Laird and Haymet [10] showed that truncating the expansion beyond the ‘ring’ term was a viable approximation up to moderate solution concentrations. The DHLL values of $S^{(2)}$ and S_{ring} are

$$S^{(2)} = -\frac{\kappa^3}{32\pi\rho}, \quad (32)$$

and

$$S_{\text{ring}} = -\frac{\kappa^3}{96\pi\rho} \quad (33)$$

with their sum giving the correct DHLL value of

$$S^{(\text{ex})} = -\frac{\kappa^3}{24\pi\rho}. \quad (34)$$

Retention of S_{ring} in equation (20) is thus required to give the requisite DHLL value [10]. These DHLL expressions are linear with respect to \sqrt{c} , and at a given concentration, depend only on the ionic valency, being independent of ionic size.

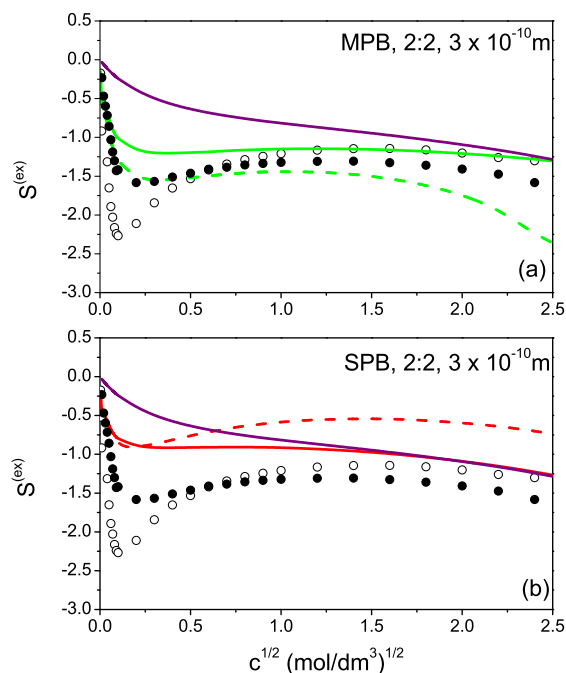


Figure 4. (Colour online) Excess entropy $S^{(\text{ex})}$ as a function of the square root of electrolyte concentration in a 2:2 valency RPM electrolyte, $d = 3 \times 10^{-10}$ m. Legend: panel (a) MPB_{TI} (solid green lines), MPB_{LH} (dashed green lines), MSA_{TI} (purple line), MC_{TI} (black filled circles), and MC_{LH} (black open circles). Panel (b) SPB_{TI} (solid red lines), SPB_{LH} (dashed red lines), MSA_{TI} (purple line), MC_{TI} (black filled circles), and MC_{LH} (black open circles). The remaining RPM parameters as in figure 1.

3. Results and discussion

In the theoretical SPB, MPB, and MSA calculations, and in the MC simulations, we have used the following physical parameters for the RPM electrolyte. Two different values for the common diameter of the ions were taken, 3×10^{-10} m and 4.25×10^{-10} m. Previously, we had worked with the latter value, which to some extent takes into account the hydration of ions. However, the smaller diameter of the ion results in an almost 3-fold reduction in the volume of the ion, which translates into a decrease in steric interactions. To assess the effect of interionic electrostatic interactions on the entropy, we have also used two different valencies, 1:1 and 2:2, respectively. A 2-fold increase in the charge of an ion is accompanied by a 4-fold increase in electrostatic interactions. Thus, we have four all symmetric electrolyte models that differ in ionic diameter and in ionic valency. In model A, the diameter was $d = 4.25 \times 10^{-10}$ m and the valency $Z = \pm 1$. In model B: $d = 4.25 \times 10^{-10}$ m, $Z = \pm 2$, in C: $d = 3 \times 10^{-10}$ m, $Z = \pm 1$, and in D: $d = 3 \times 10^{-10}$ m, $Z = \pm 2$. The theoretical calculations and the simulations were performed for 27 electrolyte concentrations ranging from $c = 0.0001$ mol/dm³ to $c = 6.76$ mol/dm³.

A basic quantity in our research is the radial distribution function $g_{ij}(r)$ and so we begin this discussion by illustrating some structural results manifest through $g_{ij}(r)$ at some selected concentrations. Figure 1 shows the SPB and MPB distribution functions at $c = 1.96$ mol/dm³, while the symbols refer to the MC data. The figure is for a RPM system with $d = 4.25 \times 10^{-10}$ m, and 1:1 valency (upper panel) and 2:2 valency (lower panel), respectively. The thickness of the ionic atmosphere is over three times the ion diameter with the MC and MPB ionic profiles $g_{ij}(r)$ displaying damped oscillations for both the systems. Although the damped oscillations for the 1:1 case are relatively faint, they are quite substantial for the higher 2:2 valency case. Such damped oscillations are typical of charged fluid systems. In electric double layers, they can lead to overcharging of the electrode. At this high concentration, the MPB profiles are still closely following their MC counterparts. However, the mean field SPB theory does not capture this

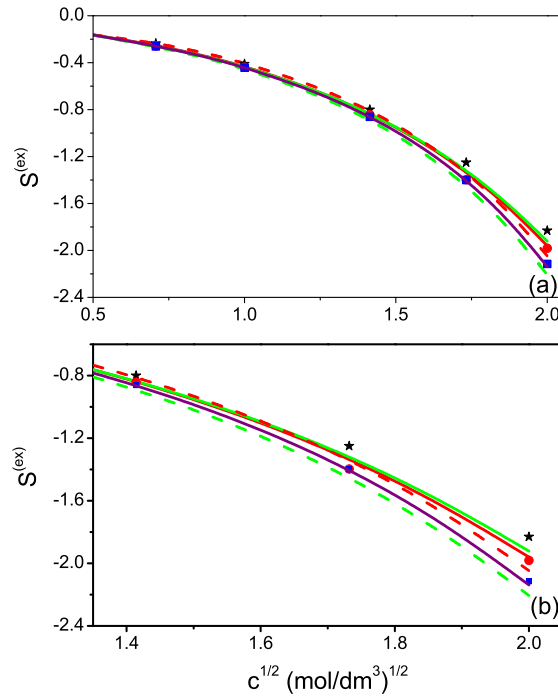


Figure 5. (Colour online) Excess entropy $S^{(ex)}$ as a function of the square root of an electrolyte concentration for a 1 : 1 RPM electrolyte, $d = 4.9 \times 10^{-10}$ m, $T = 298$ K, and $\epsilon_r = 78.356$. Legend: SPB_{TI} (solid red line), MPB_{TI} (solid green line), SPB_{LH} (dashed red line), MPB_{LH} (dashed green line), reference [4] (4th column of table IV) (black stars), reference [4] (MC Widom) (red filled circles), reference [4] (HNC) (blue squares). Panel (a) $c^{1/2}$ ranges from 0.5 $(\text{mol}/\text{dm}^3)^{1/2}$ to 2 $(\text{mol}/\text{dm}^3)^{1/2}$, panel (b) $c^{1/2}$ ranges from 1.35 $(\text{mol}/\text{dm}^3)^{1/2}$ to 2 $(\text{mol}/\text{dm}^3)^{1/2}$.

effect with the SPB $g_{ij}(r)$ being monotonously decreasing and are thus not qualitative. The behaviour of the $g_{ij}(r)$ for the other two models involving $d = 3 \times 10^{-10}$ m are not shown as they show similar trends to $d = 4.25 \times 10^{-10}$ m.

In figures 2–4 we show the TI results for the excess entropy $S^{(ex)}$ as function of \sqrt{c} from the SPB , MPB , MSA , and MC along with the corresponding results from the LH approximations. To avoid confusion, we use the notation X_{TI} and X_{LH} to denote the two cases where X stands for SPB , MPB , MSA , or MC . Figure 2 illustrates the MPB_{TI} (green curves), MPB_{LH} (green dashed curves), MC_{TI} (black filled circles), and MC_{LH} (black open circles) for a 1:1 electrolyte at $d = 4.25 \times 10^{-10}$ m (upper panel) and $d = 3 \times 10^{-10}$ m (lower panel). As can be seen, in either case, the curves and the symbols are remarkably consistent with each other with hardly any visible difference among them. The corresponding SPB and MSA curves lie on top of the MPB curves and are hence not displayed. We thus have that for the 1:1 valency (models A and C), the theories are capable of predicting the simulation data almost quantitatively up to a fairly high concentration.

The situation changes substantially in figures 3 and 4, which show the $S^{(ex)}$ for the 2:2 valencies at $d = 4.25 \times 10^{-10}$ m and $d = 3 \times 10^{-10}$ m, respectively. Although in figure 3 the theories are still broadly qualitative, the SPB_{LH} and MPB_{LH} now reveal discrepancies from the simulation data, especially at higher concentrations. With the exception of the MSA_{TI} , the theories and the MC_{TI} , MC_{LH} reveal a plateau around $c \sim 0.06$ mol/dm^3 . The MSA_{TI} curve, on the other hand, decreases monotonously. Some differences between the two sets of MC data also emerge at higher concentrations. This is possibly due to the approximations in the LH entropy expansion scheme since the same $g_{ij}(r)$'s are used in the two cases. The picture changes again in figure 4 at $d = 3 \times 10^{-10}$ m, where the MC_{LH} shows a deep minimum at low concentration (around $c \sim 0.002$ mol/dm^3 , while the MC_{TI} , SPB_{TI} , SPB_{LH} , MPB_{TI} , MPB_{LH}

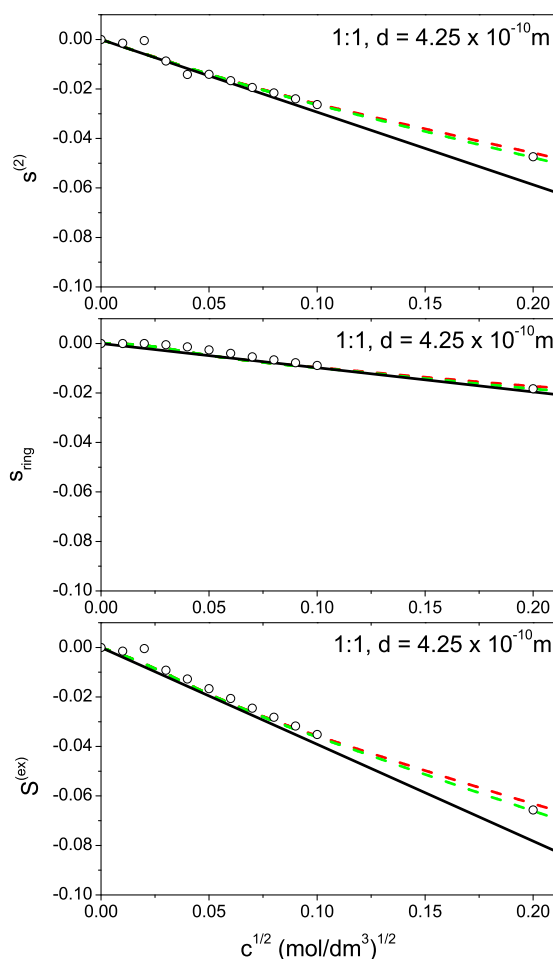


Figure 6. (Colour online) Excess entropy $S^{(ex)}$, and its components, $S^{(2)}$, and, S_{ring} , as functions of the square root of electrolyte concentration for a 1:1 RPM electrolyte with ion diameter $d = 4.25 \times 10^{-10}$ m at a low concentration regime. Legend: SPB_{LH} (dashed red lines), MPB_{LH} (dashed green lines), and MC_{LH} (black open circles). DHLL (solid black line). The rest of the physical parameters as in figure 1.

have a shallow minimum. The MSA_{TI} continues to be monotonously decreasing as in figure 3. It is likely that a simultaneous increase in Coulombic interactions and a decrease in steric interactions lead to a less random distribution of particles at very low concentrations and hence to a decrease in entropy. The MPB does not give the $d = 0$ (zero ion size) limiting behaviour at low concentrations [37, 38], while for the planar electric double layer it was suggested that the MPB decreases in accuracy as the ion diameter is reduced [39]. Although perhaps not being the reason for the apparent “poor” behaviour for 2:2, it is an indication that the MPB loses accuracy as ion size decreases at low concentrations.

A fundamental reason for the different dispositions of the TI and LH results for the $S^{(ex)}$ for the SPB, MPB, and MC in figures 2–4 can be traced back to the behaviour of the corresponding predicted $g_{ij}(r)$ vis-à-vis those of the simulations. For instance, in figure 1 at a fairly high $c = 1.96$ mol/dm³, we saw that for 1:1 valency case the SPB and the MPB profiles are quite reasonable relative to the simulations but for 2:2 valency case there are discrepancies with the SPB, in particular, not being qualitative. Such trends are likely to accentuate at still higher concentrations. This is manifested in the $S^{(ex)}$ results in these figures. In figure 2 (1:1 case) the MC_{TI} and MC_{LH} are virtually indistinguishable. The MPB_{LH} underestimates the simulations at very high concentrations (which may be attributed to the deviations in the MPB profiles) and remain below the MPB_{TI} . Two other factors that are likely to impact more the 2:2

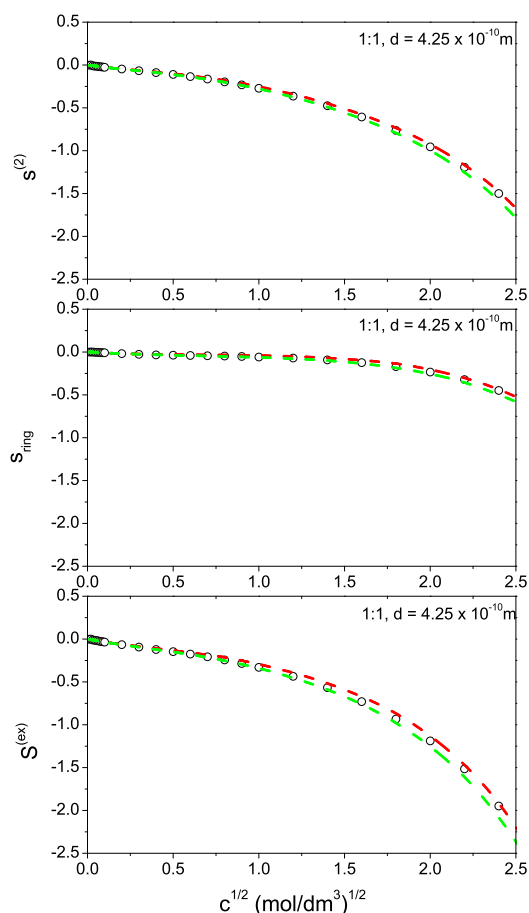


Figure 7. (Colour online) The same as figure 6, but for a broader concentration regime. DHLL not shown here.

valency results are:

- (i) the neglect of the higher order terms beyond S_{ring} in the LH expansion, and
- (ii) the fact that the U and $\phi^{(\text{ex})}$ terms in the TI expression [equation (12)]

involve only the contact values of the potential and distribution profiles, while γ_{\pm} are calculated using the Gntelberg charging process [29, 30], which gives the expression somewhat of a local character. By contrast, in evaluating the $S^{(\text{ex})}$ from the LH equations, the full range of the $g_{ij}(r)$ is necessary. This non-local nature is likely to lead to more errors.

We note here that at low concentrations for 2:2 valency cases in figures 3 and 4 the $\text{MC}_{LH} S^{(\text{ex})} < \text{MC}_{TI} S^{(\text{ex})}$. The MPB_{LH} and MPB_{TI} follow the same trend, although differing numerically from the simulation data. The SPB_{LH} and SPB_{TI} , on the other hand, reveal a different trend with $\text{SPB}_{LH} S^{(\text{ex})} > \text{SPB}_{TI} S^{(\text{ex})}$ over nearly the entire concentration region probed. The physical reason for this may well be the effect of the missing inter-ionic correlations in the classical mean field theory.

We next compare our results with one set of results for $S^{(\text{ex})}$ for bulk electrolytes available in the literature. Hummer and Soumpasis [4] calculated the $S^{(\text{ex})}$ for NaCl solutions using the RPM in conjunction with HNC integral equation theory, Widom's particle insertion MC technique, and an entropy expansion. The physical parameters used by these authors were $d = 4.9 \times 10^{-10}$ m, $\epsilon_r = 78.356$, and $T = 298$ K. In figure 5, we have plotted the entropy results at these parameters from the SPB_{TI} (solid red line), the MPB_{TI} (solid green line), the SPB_{LH} (dashed red line), and the MPB_{LH} (dashed green

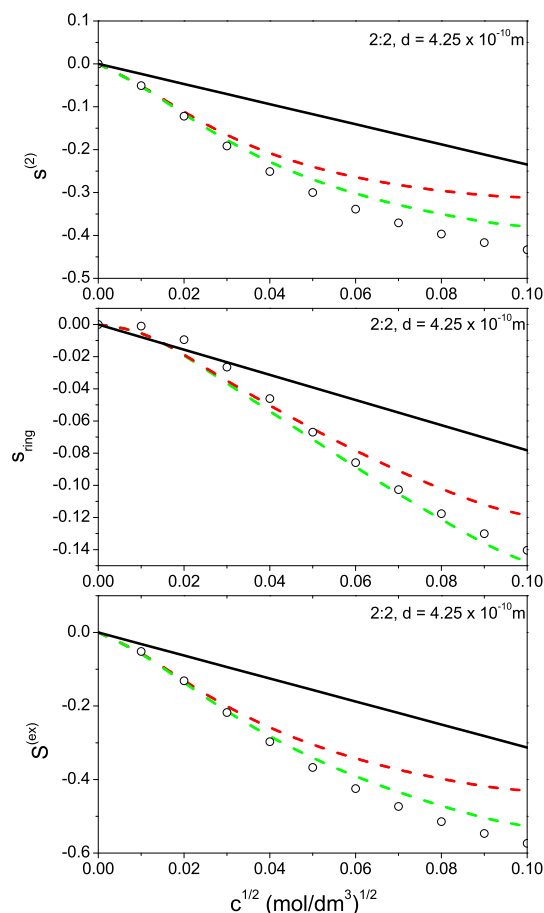


Figure 8. (Colour online) Excess entropy $S^{(\text{ex})}$ and its components, $S^{(2)}$ and S_{ring} , as functions of the square root of electrolyte concentration for a 2:2 RPM electrolyte, $d = 4.25 \times 10^{-10}$ m, at a low concentration regime. Legend: SPB_{LH} (dashed red lines), MPB_{LH} (dashed green lines), and MC_{LH} (black open circles). DHLL (solid black line). The rest of the physical parameters as in figure 1.

line) again as functions of \sqrt{c} . The Hummer-Soumpasis results from table IV of reference [4] are shown as: $s^{(2)} + s^{(3)}$ (black stars), MC (Widom) (red filled circles), and HNC (blue squares). The SPB and MPB curves compare reasonably well with the Hummer-Soumpasis data overall. The TI results from SPB and MPB are almost quantitative with their MC values. The discrepancy between the SPB_{LH} or MPB_{LH} and the $s^{(2)} + s^{(3)}$ results is most likely due to the differences in the approximations involved in the entropy expansion techniques.

In the next part of the work (figure 6–11), we examine more closely how the $g_{ij}(r)$'s for the four electrolyte models (A, B, C, and D) affect the $S^{(\text{ex})}$ as a function of \sqrt{c} . Some of the $S^{(\text{ex})}$ results for the model systems were seen in the figures 2–5, but are included here for completeness. Figure 6 shows the $S^{(\text{ex})}$ and its constituent components $S^{(2)}$ and S_{ring} for model A in the low concentration range, where the DHLL is applicable. As expected, all the DHLL curves are linear with respect to \sqrt{c} . It is not surprising that the SPB and the MPB curves together with the simulation results are also almost linear trending to the correct low concentration DHLL behaviour. Minor noise in the MC_{LH} data points are visible in the area of the lowest concentrations. This is presumably due to possible imprecision in our calculations. At such low concentrations one needs to evaluate the $g_{ij}(r)$'s around an ion out to very large distances, which can be challenging numerically. The magnitude of the S_{ring} component of the $S^{(\text{ex})}$ is much smaller than the magnitude of the $S^{(2)}$ component. The lowest entropy values are predicted by the DHLL theory followed by the MPB, MC and SPB. The results for a wider range of concentrations are shown in figure 7

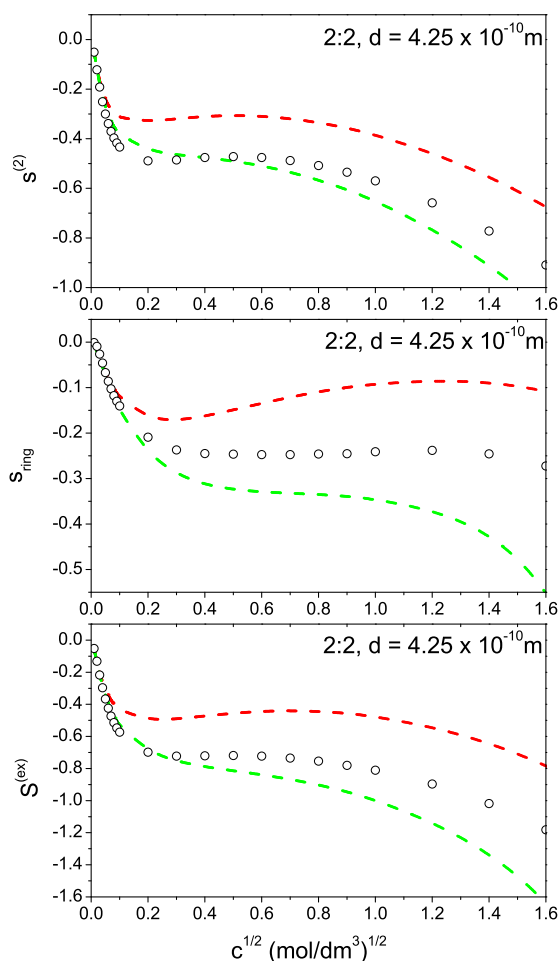


Figure 9. (Colour online) The same as figure 8, but for a broader concentration regime. DHLL not shown here.

without DHLL. The remaining curves are no longer linear with the theories still being in good agreement with the simulations. Starting from a value of $c \sim 1 \text{ mol/dm}^3$, a substantial decrease in $S^{(\text{ex})}$ and in its components is visible, with the same ordering of the curves and symbols to the entropy as in figure 6.

In model B, the ionic valency increases relative to that in model A. The results for model B are shown in figures 8 and 9, at low and high concentrations, respectively. Figure 8 reveals that even in the low concentration regime, the curves, with the exception of the DHLL, are not linear. The $S^{(2)}$ and $S^{(\text{ex})}$ curves are convex, while the S_{ring} curves are initially concave becoming more linear at higher concentrations. The theories are qualitative with the simulations, although the MPB results tend to follow the MC data more closely than do the corresponding SPB results. Note though that the scales in figure 8 are expanded and the same curves appear closer together at the scales of figure 9 at low concentrations. Also in figure 9, a sharp decrease in $S^{(2)}$, S_{ring} , and $S^{(\text{ex})}$ is visible at low concentrations followed by an inflection point, after which the curves become concave. The SPB curves pass through a maximum, the MC curves have a flat plateau, and the MPB curves decrease monotonously. A similar pattern for $S^{(\text{ex})}$ for divalent ions was observed by Laird and Haymet [10]. This behavior is somewhat similar to the dependence of the logarithm of the activity coefficient on the square root of the concentration. At low concentrations, electrostatic interactions dominate, which give a negative contribution to the activity coefficient, while as the concentration increases, steric interactions start to become more relevant, which make a positive contribution. It is not difficult to locate the boundary between the regions of dominance of electrostatic and steric interactions. However, this is not the case with entropy, where both types of interactions lead to a

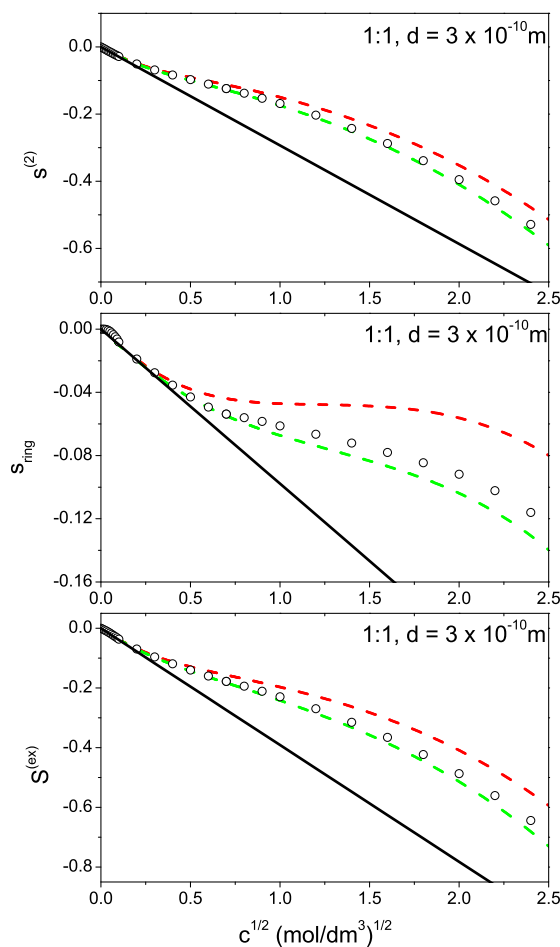


Figure 10. (Colour online) Excess entropy $S^{(\text{ex})}$ and its components $S^{(2)}$ and S_{ring} , as functions of the square root of electrolyte concentration for a 1:1 RPM electrolyte, $d = 3 \times 10^{-10}$ m. Legend: SPB_{LH} (dashed red lines), MPB_{LH} (dashed green lines), MC_{LH} (black open circles). DHLL (solid black line). The rest of the physical parameters as in figure 1.

negative contribution. This blurs the boundaries between these areas so that increasing the interactions as in model B may be helpful here. Figure 9 clearly shows three areas: predominant electrostatic interactions, transient interactions, and predominant steric interactions.

The entropy curves for model C at low electrolyte concentrations are not shown as they are very similar to those presented in figure 6 for model A. There are similarities also between the sets of curves in figure 7 (model A) and in figure 10 (model C). For instance, overall the curves follow the MC data. The MPB is semi-quantitative or better, although the SPB S_{ring} curve deviates from the simulations at higher concentrations displaying a slight hump. The other differences between the two models are: the magnitudes of the $S^{(2)}$, S_{ring} , and $S^{(\text{ex})}$ are smaller in figure 10 than in figure 7, and the S_{ring} , and $S^{(\text{ex})}$ curves have a slight inflection. This is likely caused by stronger electrostatic interactions as two ions can be at closer proximity to each other.

There is a substantial change in the panorama in going from figure 9 (model B) at $d = 4.25 \times 10^{-10}$ m to figure 11 at $d = 3 \times 10^{-10}$ m. The behaviour of the $S^{(\text{ex})}$ was explained earlier in relation to figure 4 and the TI results. Here, the MC data for both $S^{(2)}$ and S_{ring} also reveal a sharp drop at low concentrations giving a minimum. The analogous SPB and MPB curves also show a minimum, but a much shallower one. This behavior is again due to the increase in electrostatic interactions stemming from a reduced ion size compared to that in model B. The increase in concentration leads to the appearance of a flat hump.

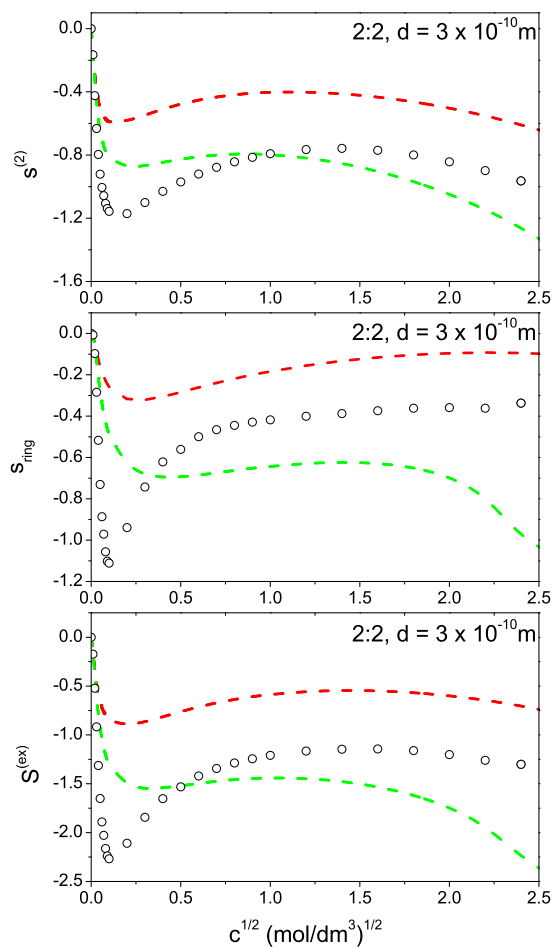


Figure 11. (Colour online) Excess entropy $S^{(ex)}$ and its components $S^{(2)}$ and S_{ring} , as functions of the square root of electrolyte concentration for a 2:2 RPM electrolyte, $d = 3 \times 10^{-10}$ m. Legend: SPB_{LH} (dashed red lines), MPB_{LH} (dashed green lines), and MC_{LH} (black open circles). DHLL (solid black line). The rest of the physical parameters as in figure 1.

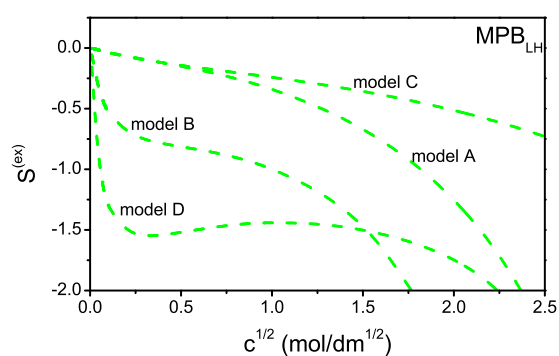


Figure 12. (Colour online) Excess entropy $S^{(ex)}$ as a function of the square root of electrolyte concentration using the MPB_{LH} for the models A, B, C, and D.

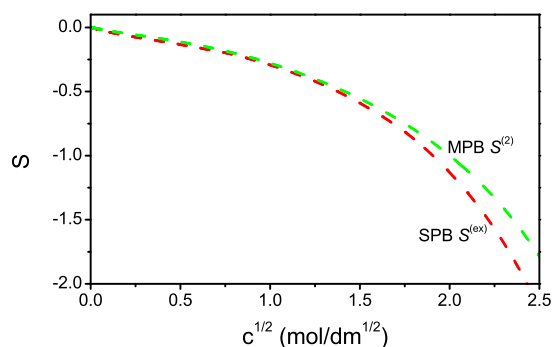


Figure 13. (Colour online) Comparison of the excess entropy, $S^{(\text{ex})}$, from the SPB theory with the $S^{(2)}$ component from the MPB theory as functions of the square root of electrolyte concentration. The physical parameters are from model A. Legend: SPB (red dashed line), MPB (dashed green line).

Subsequently, all the curves show a downward trend.

Figure 12 allows us to view the results from the point of view of steric interactions. For example, models A and C differ in the size of the ions with model A having the larger ions. This results in the $S^{(\text{ex})}$ curves of model A are running below those in C. In the case of models B and D, the picture is less clear. It is obscured by strong inter-ion electrostatic interactions. However, in the lower right corner one can still observe that the curves for B begin to decline faster than those for D, which is clearly due to greater steric interactions. The above analysis is based on the results obtained from MPB. Analogous conclusions can be reached when analyzing the results of SPB and MC.

Finally, it is interesting to note that the inclusion of fluctuation terms in the MPB theory vis-à-vis the ring approximation in the LH equations can have similar consequences. For example, figure 13 shows (for model A) the $S^{(\text{ex})}$ obtained from the SPB theory and the $S^{(2)}$ component obtained from the MPB theory as functions of \sqrt{c} . Note that the SPB curve includes the ring approximation rather than the fluctuation terms, while the MPB curve includes the fluctuation terms rather than the ring approximation. Both curves are very similar to each other.

4. Conclusions

The achievement of this paper has been an attempt to explore the statistical mechanical, potential approaches of SPB and MPB theories to calculate the entropy of RPM electrolytes on the basis of (a) thermodynamic integration, and (b) the LH equations [7, 10].

Although for charged fluids entropy is as important a thermodynamic variable as the osmotic and activity coefficients are, calculation of the entropy has received relatively less attention perhaps because of the issues involved in such calculations. From a theoretical perspective, an estimation of fluid entropy necessitates a knowledge of the distribution functions to all orders, which is a difficult task. Besides the thermodynamic integration, the LH entropy expansion suggests a way forward by an approximation that partially accounts for the contribution of higher order distributions. Thus, only the second order distribution, that is, the pair-correlation or pair distribution function, which is standard staple of any formal theory, is needed explicitly. The earlier application of the LH procedure [10] involved an electrolyte model with a soft repulsive core — not quite the primitive model.

The work here shows that overall for the RPM the SPB results for $S^{(\text{ex})}$ are generally qualitative with that from the simulations at lower concentrations, while the MPB results are semi-quantitative or better. Such trends are consistent with the SPB and MPB characterizations of thermodynamics, for instance, osmotic and activity coefficients of primitive model electrolytes vis-à-vis the corresponding simulations results reported earlier in the literature [18, 19]. Furthermore, the results from these potential based theories at $d = 4.25 \times 10^{-10}$ m for both 1:1 and 2:2 valencies show many similar characteristics as that from the integral equation theory used by Laird and Haymet [10], although the electrolyte models are not

identical. The SPB and MPB formalisms together with thermodynamic integration or LH equations are also seen to reproduce well some excess entropy results of Hummer and Soumpasis [4] obtained using a MC Widom particle insertion method, the HNC integral equation, and an entropy expansion.

An aspect of this work has been comparing the LH expansion results for the $S^{(\text{ex})}$, evaluated by the MC radial distribution functions, with that found by TI via simulation. For 1:1 electrolytes, the agreement between the two approaches is excellent, with $MC_{TI} \approx MC_{LH}$. Deficiencies between the two approaches arise, however, in the 2:2 case. For low concentrations with $d = 4.25 \times 10^{-10}$ m, the LH expansion is fairly reasonable and is qualitatively correct at the higher concentrations. With $d = 3 \times 10^{-10}$ m the LH scheme is inappropriate at low concentrations and is only qualitatively correct at higher concentrations.

The thermodynamic properties of 1:1 and 2:2 salts differ due to the strong interionic forces for higher charges. Examples include the negative deviation of the 2:2 electrolyte mean activity coefficient from the DHLL at high dilution, compared to the positive deviation for the 1:1 case, with an analogous behaviour for the osmotic coefficient [40–42]. Bjerrum [43] introduced the idea of ion pairs which has provided the inspiration for many a theoretical investigation involving ionic association [44, 45]. Support for ion association has been given by integral equation theories, although the unmodified HNC theory overestimates the pair and triple aggregates [46, 47]. It thus seems that ionic association is playing a fairly significant role in the initial rapid decrease in $S^{(\text{ex})}$ at high dilution seen in figures 3 and 4, the smaller radius leading to a deep minimum. The MPB accurately predicts the RPM 2:2 thermodynamic and structural simulation results at $d = 4.25 \times 10^{-10}$ m, with its accuracy reducing as d decreases, as well as those predictions related to the classical approach at low concentrations [48]. The SPB is less successful than the MPB in predicting $S^{(\text{ex})}$. As the MPB includes fluctuation terms, the interpretation of ionic association can be ascribed to the addition of fluctuation terms into the mean field SPB theory. The contribution of higher terms in the LH expansion is difficult to assess as these terms contain multi-particle correlation functions. As indicated in the previous Section, for the 1:1 case at the treated parameters, the comparison of the MC_{TI} and MC_{LH} data in figure 2 indicate that these higher terms make a small or negligible contribution. Deviations occur between the simulation results for 2:2 electrolytes. At $d = 4.25 \times 10^{-10}$ m, the MC_{TI} and MC_{LH} diverge at the higher concentrations, while with $d = 3 \times 10^{-10}$ m, the difference persists throughout the concentration range and can be very pronounced (figure 4). The neglect of the higher order terms in the LH theory for 2:2 electrolytes can be interpreted as leading to an increase in ion association, as ion size reduces, at high dilution.

Within the present formulation of the SPB theory, it might be feasible to incorporate a soft core potential. The g_{ij}^0 would need to be replaced by the corresponding quantity for a soft potential. In case of the MPB, however, the $L_i(u_j)$ also depends on the ion-size. Another possible extension of the present work can be envisaged through the use of a variable dielectric constant. The dependence of the ϵ_r on the solution concentration and/or temperature is an experimental phenomenon [44]. Some of us were involved earlier in a thermodynamic analysis of some alkali halide solutions with a concentration or temperature dependent ϵ_r using the SPB, MPB, and the MSA with encouraging results [19]. We hope to build on the present study along these lines in future.

Acknowledgements

Professor Stanisław Lamperski passed away before the paper was completed. He conceived and carried out the majority of the computations, which were kindly finished by Dr. Rafał Gorniak. We acknowledge financial support to Professor Lamperski from Adam Mickiewicz University, Poznań, Poland.

References

1. Boltzmann L., Sitzungsbetichte der Kaiserlichen Akademie der Wissenschaften Mathematisch-Naturwissen Classe. Part II, Vol. LXXVI.76, 1877, 373.
2. Gibbs J. W., Am. J. Sci., 1878, **s3-16**, 1875–1978, doi:10.2475/ajs.s3-16.96.441.
3. Shannon C. E., Bell Syst. Tech. J., 1948, **27**, 379–423, doi:10.1002/j.1538-7305.1948.tb01338.x.
4. Hummer G., Soumpasis D. K., J. Chem. Phys., 1993, **98**, 581, doi:10.1021/jp951011v.
5. McQuarrie D. A., Statistical Mechanics, Harper and Row, New York, 1976.

6. Green H. S., *Molecular Theory of Liquids*, North-Holland, Amsterdam, 1952.
7. Laird B. B., Haymet A. D. J., *Phys. Rev. A*, 1992, **45**, 5680, doi:10.1103/PhysRevA.45.5680.
8. Hernando J. A., *Mol. Phys.*, 1990, **69**, 319, doi:10.1080/00268979000100211.
9. Hernando J. A., *Mol. Phys.*, 1990, **69**, 327, doi:10.1080/00268979000100221.
10. Laird B. B., Haymet A. D. J., *J. Chem. Phys.*, 1994, **100**, 3775, doi:10.1063/1.466365.
11. Silverstein K. A. T., Dill K. A., Haymet A. D. J., *J. Chem. Phys.*, 2001, **114**, 6303, doi:10.1063/1.1355997.
12. Lazaridis T., *J. Phys. Chem. B*, 1998, **102**, 3531, doi:10.1021/jp9723574.
13. Lazaridis T., Karplus M., *J. Chem. Phys.*, 1996, **105**, 4294, doi:10.1063/1.472247.
14. Hernando J. A., Blum L., *Phys. Rev. E*, 2000, **62**, 6577, doi:10.1103/PhysRevE.62.6577.
15. Laird B. B., Wang J., Haymet A. D. J., *Phys. Rev. E*, 1993, **47**, 2491, doi:10.1103/PhysRevE.47.2491.
16. Laird B. B., Wang J., Haymet A. D. J., *Phys. Rev. E*, 1993, **48**, 4145, doi:10.1103/PhysRevE.48.4145.
17. Outhwaite C. W., In: *Statistical Mechanics*, Vol. 2, Singer K. (Ed.), The Royal Society of Chemistry, first edn., 1975, 188–255, doi:10.1039/9781847556936-00188.
18. Quiñones A. O., Bhuiyan L. B., Abbas Z., Outhwaite C. W., *Condens. Matter Phys.*, 2018, **21**, 23802, doi:10.5488/CMP.21.23802.
19. Quiñones A. O., Bhuiyan L. B., Abbas Z., Outhwaite C. W., *J. Mol. Liq.*, 2023, **371**, 12119, doi:10.1016/j.molliq.2022.121119.
20. Molero M., Outhwaite C. W., Bhuiyan L. B., *J. Mol. Liq.*, 2023, **390**, 123025, doi:10.1016/j.molliq.2023.123025.
21. Molero M., Outhwaite C. W., Bhuiyan L. B., *Phys. Chem. Chem. Phys.*, 2024, **26**, 10029, doi:10.1039/D3CP05808E.
22. Ruas A., Moisy P., Simonin J.-P., Bernard O., Dufreche J.-F., Turq P., *J. Phys. Chem. B*, 2005, **109**, 5243, doi:10.1021/jp0450991.
23. Blum L., *Mol. Phys.*, 1975, **30**, 1529, doi:10.1080/00268977500103051.
24. Høye J. S., Blum L., *Mol. Phys.*, 1978, **78**, 299, doi:10.1080/00268977800100221.
25. Sanchez-Castro C., Blum L., *J. Phys. Chem. B*, 1989, **93**, 7478, doi:10.1021/j100358a043.
26. Outhwaite C. W., *Chem. Phys. Lett.*, 1978, **53**, 599, doi:10.1016/0009-2614(78)80078-5.
27. Outhwaite C. W., *J. Chem. Soc., Faraday Trans. 2*, 1987, **83**, 949, doi:10.1039/F29878300949.
28. Outhwaite C. W., Molero M., Bhuiyan L. B., *J. Chem. Soc., Faraday Trans.*, 1991, **87**, 3227, doi:10.1039/FT9918703227.
29. Outhwaite C. W., Molero M., Bhuiyan L. B., *J. Chem. Soc., Faraday Trans.*, 1993, **89**, 1315, doi:10.1039/FT9938901315.
30. Outhwaite C. W., Molero M., Bhuiyan L. B., *J. Chem. Soc. Faraday Trans.*, 1994, **90**, 2002, doi:10.1039/FT9949002001.
31. Outhwaite C. W., *Condens. Matter Phys.*, 2004, **7**, 719, doi:10.5488/CMP.7.4.719.
32. Hansen J. -P., McDonald I. R., *Theory of Simple Liquids*, 2nd Edn., Academic Press, London, 1990.
33. Hribar Lee B., Vlachy V., Bhuiyan L. B., Outhwaite C. W., Molero M., *Mol. Phys.*, 2003, **101**, 2969, doi:10.1080/00268970310001608441.
34. Rešič J., Vlachy V., Bhuiyan L. B., Outhwaite C. W., *Langmuir*, 2004, **21**, 481, doi:10.1021/la049285+.
35. Lamperski S., *Mol. Simul.*, 2007, **33**, 1193, doi:10.1080/08927020701739493.
36. Frenkel D., Smit B., *Understanding Molecular Simulation, From Algorithms to Applications*, Academic Press, San Diego, 1996.
37. Kjellander R., Mitchell D. J., *J. Chem. Phys.*, 1994, **101**, 603, doi:10.1063/1.468116.
38. Mitchell D. J., Ninham B. W., *Chem. Phys. Lett.*, 1978, **53**, 397, doi:10.1016/0009-2614(78)85426-8.
39. Carnie S. L., Torrie G. M., Valleau J. P., *Mol. Phys.*, 1984, **53**, 253, doi:10.1080/00268978400102261.
40. Harned H. S., Owen B. B., *The Physical Chemistry of Electrolyte Solutions*, 3rd ed., Reinhold, New York, 1958.
41. Robinson R. A., Stokes R. H., *Electrolyte Solutions*, 2nd ed., Dover, New York, 2002.
42. Guggenheim E. A., Stokes R. H., *The International Encyclopedia of Physical Chemistry and Chemical Physics*, Vol. 1, Equilibrium Properties of Aqueous Solutions of Single Strong Electrolytes, Pergamon Press, Oxford, 1969.
43. Bjerrum N., Dansk K., *Videnskab. Selskab, Math.-Fys. Medd.*, 1926, **7**, 1.
44. Barthel J., Krienke H., Kunz W., *Physical Chemistry of Electrolyte Solutions: Modern Aspects*, Topics in Physical Chemistry, Vol. 5, Springer, New York, 1998.
45. Holovko M., In: *Ionic Soft Matter: Modern Trends in Theory and Applications*, Henderson D., Holovko M., Trokhymchuk A. (Eds.), NATO Science Series II. Mathematics, Physics and Chemistry, Vol. 206, Springer, Dordrecht, 2005.
46. Rossky P. J., Dudowicz J. B., Tembe B. L., Friedman H. L., *J. Chem. Phys.*, 1980, **73**, 3372, doi:10.1063/1.440533.
47. Rogde S. A., Hafskjold B., *Mol. Phys.*, 1983, **48**, 1241, doi:10.1080/00268978300100891.
48. Malatesta F., *J. Solution Chem.*, 2020, **49**, 1536, doi:10.1007/s10953-01041-8.

Ентропія електроліту в рамках обмеженої примітивної моделі з використанням підходу середнього електростатичного потенціалу

С. Ламперскі¹, Л. Б. Буян², К. В. Оутвайт³, Р. Горняк¹

¹ Хімічний факультет, Університет імені Адама Міцкевича, вул. Познанського університету, 8, 61-614 Познань, Польща

² Лабораторія теоретичної фізики, Фізичний факультет, Університет Пуерто-Ріко

³ Вища школа математики та фізики, університет Шеффілда, Шеффілд S3 7RH, Великобританія

Надлишкова ентропія електролітів в рамках обмеженої примітивної моделі розраховується з використанням методу потенціалу за допомогою симетричної теорії Пуассона-Больцмана та модифікованої теорії Пуассона-Больцмана. Ці теоретичні підходи використовуються у поєднанні з рівняннями статистичної термодинаміки, яке, як показано, є еквівалентним термодинамічному інтегруванню. Системи електролітів з іонними валентностями 1:1 і 2:2 та з діаметрами 3×10^{-10} м і $4,25 \times 10^{-10}$ м розглядаються в широкому діапазоні концентрацій. Точні радіальні функції розподілу для модельних електролітів, отримані в результаті моделювання Монте-Карло в канонічному ансамблі, порівнюються з відповідними теоретичними передбаченнями. Крім того, функції радіального розподілу, отримані як теоретичним чином так і методом моделювання, використовуються в рівняннях розкладу ентропії Лейрда-Хаймета [J. Chem. Phys., 1994, **100**, 3775] для оцінки надлишкової ентропії розчинів. Ці рівняння враховують багаточастинкові функції розподілу, які апроксимуються за допомогою "кільцевого" доданка. Загалом, модифікована теорія Пуассона-Больцмана дає результати, які більш узгоджуються з даними моделювання, ніж з результати симетричної теорії Пуассона-Больцмана. Отримані результати показують, що надлишкова ентропія є від'ємною, а її абсолютне значення зростає для електролітів 1:1 зі збільшенням концентрації. Симетричні значення Пуассона-Больцмана дещо завищені, а модифіковані значення Пуассона-Больцмана дещо занижені у порівнянні з модельними. Криві для електролітів 1:1 включно з кривими, отриманими з рівнянь Лейрда-Хаймета, узгоджуються одна з одною, тоді як криві для електролітів 2:2 при $4,25 \times 10^{-10}$ м, отримані в рамках модифікованої теорії Пуассона-Больцмана, лише якісно узгоджуються з даними моделювання до густин 1 моль/дм³. Криві для електролітів 2:2 мають характерний перегин і плато. Результати, отримані в діапазоні низьких концентрацій ($< 0,01$ моль/дм³), узгоджуються з передбаченнями закону Дебая-Гюккеля.

Ключові слова: електроліти, обмежена примітивна модель, ентропія, термодинамічне інтегрування, метод Монте-Карло, симетризовані модифіковані теорії Пуассона-Больцмана